Rolled-Up Three-Dimensional Metamaterials with a Tunable Plasma Frequency in the Visible Regime

Stephan Schwaiger, Markus Bröll, Andreas Krohn, Andrea Stemmann, Christian Heyn, Yuliya Stark, Daniel Stickler, Detlef Heitmann, and Stefan Mendach*

Institut für Angewandte Physik und Zentrum für Mikrostrukturforschung, Universität Hamburg, Jungiusstrasse 11, D-20355 Hamburg, Germany

(Received 20 October 2008; revised manuscript received 30 January 2009; published 24 April 2009)

We propose and realize a novel concept of a self-organized three-dimensional metamaterial with a plasma frequency in the visible regime. We utilize the concept of self-rolling strained layers to roll up InGaAs/GaAs/Ag multilayers with multiple rotations. The walls of the resulting tubes represent a radial superlattice with a tunable layer thickness ratio and lattice constant. We show that the plasma frequency of the radial superlattice can be tuned over a broad range in the visible and near infrared by changing the layer thickness ratio in good agreement with an effective metamaterial description. Finite difference time domain simulations reveal that the rolled-up radial superlattices can be used as hyperlenses in the visible.

DOI: 10.1103/PhysRevLett.102.163903 PACS numbers: 42.70.−a, 78.67.−n

Metamaterials based on artificial building blocks with a size and lattice constant smaller than the wavelength of the transmitted electromagnetic waves have gained considerable interest in the science community since the beginning of this century. Many new effects, e.g., negative refraction, superlensing, or object cloaking, have been demonstrated for metamaterials working in the microwave regime [1–5]. To explore the visible regime it is required that the artificial building blocks be scaled down to the order of 100 nm. Commonly planar lithographic techniques are used to obtain such small dimensions [6–8]. To construct three-dimensional materials, the planar processing step is repeated until the desired thickness is obtained [9,10]. Hyperlenses [11,12] for ultraviolet light have been created by using this sequential method for alternating layers of Ag and Al_2O_3 [13]. Recent alternative approaches for three-dimensional metamaterials in the visible are based on direct laser writing [14] and atomic layer deposition [15].

In this Letter we show that the concept of self-rolling strained multilayers [16,17] can be utilized to create three-dimensional metamaterials by rolling up planar metal and semiconductor films with multiple rotations. The walls of the resulting tubes represent high quality three-dimensional radial superlattices (RSLs) with accurately tunable unit cells and lattice constants [18,19]. We perform transmission measurements on RSLs which consist of (In)GaAs and Ag [Fig. 1(b)] and explain our results within the framework of an effective metamaterial approximation. We demonstrate that the effective plasma frequency of the RSLs can be shifted over a broad range in the visible and near infrared by changing the ratio between Ag and (In) GaAs layer thickness. By means of finite difference time domain simulations we show that our RSLs might be used as hollow fluid fillable [20] hyperlenses working in this frequency regime.

The RSLs are prepared as follows: Initially a GaAs buffer layer (100 nm) is grown on a GaAs substrate using molecular beam epitaxy, followed by an AlAs sacrificial layer (40 nm), a strained $In_{20}Ga_{80}As$ layer (17 nm), and a GaAs layer (17 nm). Subsequently an Ag layer is deposited on the semiconductor by thermal evaporation. In this work we varied the Ag layer thickness for different samples between 17 and 25 nm. The exact thickness of the Ag layers was measured with an atomic force microscope. The strained layer system is released from the substrate by selectively etching away the AlAs sacrificial layer and minimizes its strain energy by rolling up into a tube. Details of the lithographic process used can be found in Ref. [21]. In good agreement with continuum strain theory [22] we obtain outer tube radii of $r_{\mathrm{tube}} = 2\ \mu$m to $r_{\mathrm{tube}} = 3\ \mu$m [Fig. 1(a)].

For transmission measurements through the tube walls we developed a transmission setup as shown in Fig. 2(a). To realize a light source which can be placed inside the microtubes we use a tapered multimode glass fiber with a core diameter of 65 μm and a tip diameter of less

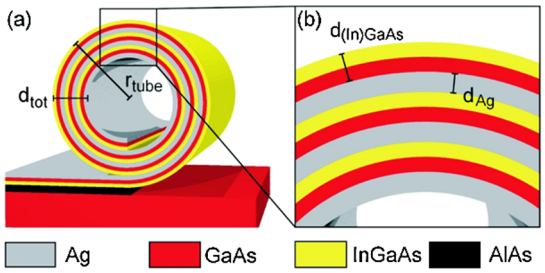

FIG. 1 (color online). (a) Sketch of the microtube. The AlAs sacrificial layer is removed by selective etching. The released strained multilayer of $In_{20}Ga_{80}As/GaAs/Ag$ relaxes and rolls up into a microtube. (b) The wall of the tube represents a RSL that consists of alternating layers of metal and semiconductor.

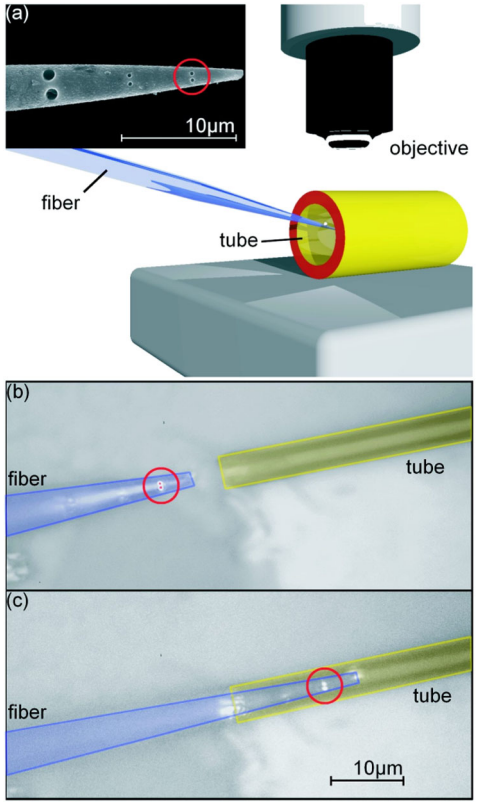

FIG. 2 (color online). (a) Scanning electron microscope image of the tip of the fiber and sketch of the setup. The patterns in the tip metallization are prepared by focused ion beams. The fiber is manipulated by an XYZ piezostack. The signal is collected by a microscope objective and measured with a CCD. Intensity measurements on selected areas (cf. red circle) are performed using software based apertures. (b) Microscope image of the fiber in front of the microtube. The light, which is coupled into the fiber, is scattered through the holes in the tip metallization (red circle). (c) The fiber tip is manipulated into the microtube, and the light is transmitted through the RSL.

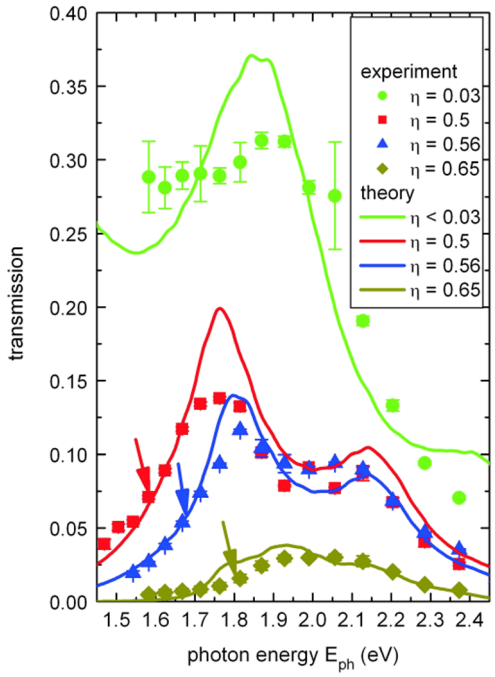

FIG. 3 (color online). Measured transmission data (symbols) of an (In)GaAs/Ag radial superlattice together with the corresponding transfer matrix calculations for perpendicular incidence on a flat multilayer (solid lines). For most data points the error bars are smaller than the symbols. The thickness of the InGaAs/GaAs layer was $d_{(\mathrm{In})\mathrm{GaAs}} = 34$ nm for all samples, and the Ag-layer thickness was varied. Circles, $\eta < 0.03$ ($d_{\mathrm{Ag}} < 1$ nm) with 5 rotations and $d_{\mathrm{tot}} \approx 170$ nm; squares, $\eta = 0.5$ ($d_{\mathrm{Ag}} = 17$ nm) with 4 rotations and $d_{\mathrm{tot}} = 204$ nm; triangles, $\eta = 0.56$ ($d_{\mathrm{Ag}} = 19$ nm) with 4 rotations and $d_{\mathrm{tot}} = 212$ nm; rhombuses, $\eta = 0.65$ ($d_{\mathrm{Ag}} = 22$ nm) with 6 rotations and $d_{\mathrm{tot}} = 336$ nm. The arrows point to the center of the respective plasma edge (cf. Fig. 4).

than 1 μm. The tip is metallized with 50–100 nm Al and patterned using a focused ion beam. As shown in Fig. 2 the holes patterned into the fiber tip metallization represent well-defined point sources. The fiber is mounted on an XYZ piezostage and can be positioned with an accuracy of approximately 100 nm. The light of a supercontiuum light source (Koheras A/S—Compact) is passed through a monochromator and coupled into the fiber. We collect the light with a 100× objective and detect it with a CCD camera (Spiricon, Inc.—USB L230). The emission from a selected area of the image (cf. red circles in Fig. 2) can be measured using a software based aperture. A reference spectrum is taken with the fiber tip outside of the microtube [Fig. 2(b)]. Subsequently the tip is manipulated into the microtube, and the transmitted intensity is recorded [Fig. 2(c)]. Finally, a second reference spectrum is taken, again with the fiber tip outside of the microtube.

The symbols in Fig. 3 represent the measured transmission through the RSL for four samples with different layer thickness ratios $\eta = d_{\mathrm{Ag}}/d_{(\mathrm{In})\mathrm{GaAs}}$. Data points are obtained by normalizing the transmitted intensity by the average of the two reference spectra. The error bars reflect the variation of the reference spectra. The solid lines represent the corresponding transfer matrix calculations [23] for perpendicular incidence on a flat multilayer. The optical material parameters for the layers were taken from Refs. [24,25]. We find a good agreement between theory curves and experimental data. Slight deviations might be attributed to Fabry-Pérot interferences in the walls of the microtubes which are less pronounced in the real sample due to surface roughness. The thickness of the InGaAs/GaAs layer was $d_{(\mathrm{In})\mathrm{GaAs}} = 34$ nm for all samples, and the Ag-layer thickness was varied. Sample $\eta < 0.03$ ($d_{\mathrm{Ag}} < 1$ nm) is rolled up 5 times and exhibits a total thickness of $d_{\mathrm{tot}} \approx 170$ nm. Sample $\eta = 0.5$ ($d_{\mathrm{Ag}} = 17$ nm) is rolled up 4 times and exhibits a thickness of $d_{\mathrm{tot}} = 204$ nm. Sample $\eta = 0.56$ ($d_{\mathrm{Ag}} = 19$ nm) is also rolled up 4 times and is slightly thicker with a thickness of $d_{\mathrm{tot}} = 212$ nm. Sample $\eta = 0.65$ ($d_{\mathrm{Ag}} = 22$ nm) is rolled up 6 times and exhibits a thickness of $d_{\mathrm{tot}} = 336$ nm. All

samples show a decay of transmission towards high energies. The maximum of transmission of sample $\eta = 0.5$ is 14% at $E_{\mathrm{ph}} = 1.76$ eV. The maximum of transmission of sample $\eta = 0.56$ is 12% at $E_{\mathrm{ph}} = 1.81$ eV. The maximum of transmission of sample $\eta = 0.65$ is 3% at $E_{\mathrm{ph}} = 2.05$ eV. The samples $\eta = 0.5$, $\eta = 0.56$, and $\eta = 0.65$ show a decrease of transmission towards low energies.

To qualitatively understand the transmission spectra we applied, in addition to the exact transfer matrix method used above, the effective metamaterial approximation [26]. In this approximation the components of the effective permittivity parallel (ϵ_p) and perpendicular (ϵ_s) to the multilayer planes are described as

$$\epsilon_p = \frac{\epsilon_{(\mathrm{In})\mathrm{GaAs}} + \eta\epsilon_{\mathrm{Ag}}}{1+\eta}, \tag{1}$$

$$\frac{1}{\epsilon_s} = \frac{1}{1+\eta}\left(\frac{1}{\epsilon_{(\mathrm{In})\mathrm{GaAs}}} + \frac{\eta}{\epsilon_{\mathrm{Ag}}}\right). \tag{2}$$

For normal incidence only the in-plane component ϵ_p is relevant. The decrease of transmission towards high energies in our spectra is caused by a continuous increase of absorption, i.e., an increase of the imaginary part of ϵ_p, which is dominated by the imaginary part of $\epsilon_{(\mathrm{In})\mathrm{GaAs}}$ at high photon energies. In contrast to this, the decay towards low energies in the samples $\eta = 0.5$, $\eta = 0.56$, and $\eta = 0.65$ is not due to absorption. It can be identified as the plasma edge of the effective metamaterial: Below the plasma edge the real part of ϵ_p becomes negative, and the metamaterial exhibits metallic reflection. The frequency at the zero crossing of ϵ_p is the plasma frequency ω_p of the metamaterial. It depends on the layer thickness ratio η and shifts to lower frequencies with decreasing Ag-layer thickness. The plasma edge for $\eta < 0.03$ is expected in the infrared and lies outside of the measuring range of our setup. In Fig. 4 we demonstrate that the plasma frequency ω_p of our RSL metamaterial can be shifted over the visible range. The solid line gives the values of ω_p calculated with the effective metamaterial approximation, i.e., Eq. (1). The red squares are experimental values for ω_p characterized by the center position of the measured plasma edges for different η (cf. arrows in Fig. 3). A comparison of measurement and theory shows that the effective metamaterial description is a very good approximation for our RSLs. For reduced lattice constants, i.e., reduced layer thicknesses, we would expect full quantitative agreement.

In analogy to hyperlenses based on curved multilayers of Ag and Al_2O_3 with a plasma frequency in the ultraviolet range [13], our approach might be used to obtain hollow hyperlenses working in the visible. At the plasma frequency ω_p hyperlenses with $\eta \neq 1$ exhibit a pronounced anisotropy in the effective permittivity with $\epsilon_p \ll \epsilon_s$. This anisotropy leads to unidirectional propagation perpendicular to the multilayers, i.e., in radial direction (channeling), and the transmission of subwavelength details [13,26]. In

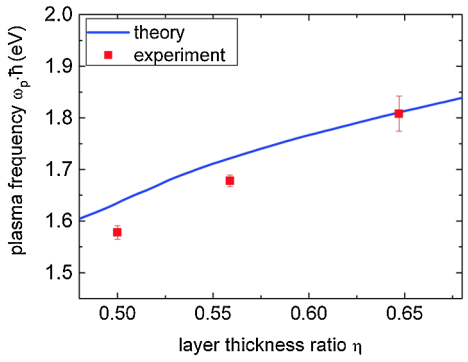

FIG. 4 (color online). Plasma frequency of RSL metamaterial with different layer thickness ratios η. The solid line gives the values of ω_p calculated with the effective metamaterial approximation, i.e., Eq. (1). The red squares are experimental values for ω_p characterized by the center position of the measured plasma edges. The uncertainty of the center position is indicated by error bars.

wave fields propagating from the inner to the outer shell of a hyperlens, subwavelength details are magnified by the ratio $V = r_{\mathrm{outer}}/r_{\mathrm{inner}}$ of the outer and the inner radius due to conservation of the angular momentum of the wave vectors [12]. In Fig. 5 we demonstrate that Ag/(In)GaAs RSLs exhibit hyperlensing at visible frequencies by means of finite difference time domain simulations (Lumerical FDTD-solutions). The optical parameters used in the simu-

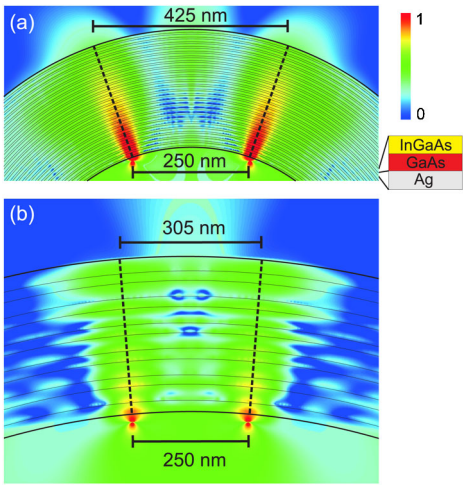

FIG. 5 (color online). Finite difference time domain simulations (Lumerical FDTD-solutions) on hyperlenses working at visible frequencies based on rolled-up Ag/(In)GaAs RSLs. Two dipoles with a distance of 250 nm are placed at the inner perimeter of the RSL. The dipoles emit at $\lambda_p = 685$ nm with H polarized along the RSL axis. The value of H_z represents the wave field normalized to the dipole sources and is given by a logarithmic color plot. (a) RSL with $\eta = 0.65$, $d_{\mathrm{Ag}} = 4$ nm, $d_{(\mathrm{In})\mathrm{GaAs}} = 6$ nm, 25 rotations, $r_{\mathrm{inner}} = 0.380$ μm, $r_{\mathrm{outer}} = 0.630$ μm, $V = 1.7$. (b) RSL with $\eta = 0.65$, $d_{\mathrm{Ag}} = 22$ nm, $d_{(\mathrm{In})\mathrm{GaAs}} = 34$ nm, six rotations, $r_{\mathrm{inner}} = 1.500$ μm, $r_{\mathrm{outer}} = 1.836$ μm, $V = 1.2$.

lations correspond to the experimental values [24,25] used for the exact transfer matrix calculations in Fig. 3. In Fig. 5(a) we show the results for a RSL with $d_{Ag} = 4$ nm and $d_{(In)GaAs} = 6$ nm ($\eta = 0.65$), 25 rotations, $r_{inner} = 0.380$ μm, and $r_{outer} = 0.630$ μm. A RSL with such a small lattice constant is technologically challenging but nevertheless feasible as it has been shown for other material systems [18]. In the simulations two dipoles with a distance of 250 nm are placed at the inner perimeter of a RSL. The dipoles emit at the plasma frequency $\omega_p = 1.8$ eV ($\lambda_p = 685$ nm) of the system with magnetic field vector H_z and electric field vector pointing along and perpendicular to the axis of the RSL, respectively. The value of H_z is indicated in a logarithmic color plot normalized to the maximum value at the dipole sources. As expected from the effective medium picture, the electromagnetic field is radially channeled, and the near field of the dipoles is transmitted from the inner to the outer parameter; i.e., the RSL exhibits hyperlensing. In the image on the outer perimeter of the RSL the distance of the dipoles is magnified from 250 to 425 nm ($V = r_{outer}/r_{inner} = 1.7$), and the full width at half maximum value of the radiation loops at the interface is 20 nm; i.e., the image is resolvable with conventional far field optics (numeric aperture >0.8) at $\lambda_p = 685$ nm. This demonstrates the feasibility of our novel hyperlens concept.

We have also performed simulations for our realized devices. Figure 5(b) shows simulations on the RSL with $d_{Ag} = 22$ nm and $d_{(In)GaAs} = 34$ nm ($\eta = 0.65$), six rotations, $r_{inner} = 1.500$ μm, $r_{outer} = 1.836$ μm. We find a magnification of the dipole distance from 250 to 305 nm ($V = r_{outer}/r_{inner} = 1.2$) and radiation loops with a full width at half maximum value of 110 nm, indicating that this device is so far not really capable of magnifying subwavelength details to the far field. Nevertheless, with further improvement of growth and preparation techniques a device as discussed in Fig. 5(a) should be realized and hyperlensing at visible frequencies possible.

In conclusion, we fabricated radial metamaterials based on self-rolling InGaAs/GaAs/Ag multilayers. We demonstrated that this novel kind of metamaterial can be described by effective parameters in a good approximation and exhibits a tunable plasma frequency in the visible range. By means of finite difference time domain simulations we showed that rolled-up InGaAs/GaAs/Ag multilayers exhibit subwavelength imaging with magnification at visible frequencies, giving rise to using them as hollow fluid fillable [20] hyperlenses. Apart from this, our approach might be used to roll up any two-dimensional metamaterial into a three-dimensional radial geometry and to realize metamaterials containing—for example, optically active—semiconductor quantum systems.

We gratefully acknowledge fruitful discussions with Nils Gerken and support by the Deutsche Forschungsgemeinschaft (DFG) via GrK 1286 and SFB 508.

*Corresponding author.
smendach@physnet.uni-hamburg.de

[1] V. G. Veselago, Sov. Phys. Usp. **10**, 509 (1968).
[2] D. R. Smith, W. J. Padilla, D. C. Vier, S. C. Nemat-Nasser, and S. Schultz, Phys. Rev. Lett. **84**, 4184 (2000).
[3] R. A. Shelby, D. R. Smith, and S. Schultz, Science **292**, 77 (2001).
[4] A. A. Houck, J. B. Brock, and I. L. Chuang, Phys. Rev. Lett. **90**, 137401 (2003).
[5] D. Schurig, J. J. Mock, B. J. Justice, S. A. Cummer, J. B. Pendry, A. F. Starr, and D. R. Smith, Science **314**, 977 (2006)
[6] S. Linden, C. Enkrich, M. Wegener, J. Zhou, T. Koschny, and C. M. Soukoulis, Science **306**, 1351 (2004).
[7] A. N. Grigorenko, A. K. Geim, H. F. Gleeson, Y. Zhang, A. A. Firsov, I. Y. Khrushchev, and J. Petrovic, Nature (London) **438**, 335 (2005).
[8] G. Dolling, C. Enkrich, M. Wegener, C. M. Soukoulis, and S. Linden, Opt. Lett. **31**, 1800 (2006).
[9] N. Liu, H. Guo, L. Fu, S. Kaiser, H. Schweizer, and H. Giessen, Nature Mater. **7**, 31 (2008).
[10] J. Valentine, S. Zhang, T. Zentgraf, E. Ulin-Avila, D. A. Genov, G. Bartal, and X. Zhang, Nature (London) **455**, 376 (2008).
[11] X. Zhang and Z. Liu, Nature Mater. **7**, 435 (2008).
[12] X. Jacob, L. V. Alekseyev, and E. Narimanov, Opt. Express **14**, 8247 (2006).
[13] Z. Liu, H. Lee, Y. Xiong, C. Sun, and X. Zhang, Science **315**, 1686 (2007).
[14] M. S. Rill, C. Plet, M. Thiel, I. Staude, G. von Freymann, S. Linden, and M. Wegener, Nature Mater. **7**, 543 (2008).
[15] J. Yao, Z. Liu, Y. Liu, Y. Wang, C. Sun, G. Bartal, A. M. Stacy, and X. Zhang, Science **321**, 930 (2008).
[16] V. Ya Prinz, V. A. Seleznev, and A. K. Gutakovsky, A. V. Chehovskiy, V. V. Preobrazhenskii, M. A. Putyato, T. A. Gavrilova, Physica E (Amsterdam) **6**, 828 (2000).
[17] O. G. Schmidt and K. Eberl, Nature (London) **410**, 168 (2001).
[18] C. Deneke, W. Sigle, U. Eigenthaler, P. A. van Aken, G. Schütz, and O. G. Schmidt, Appl. Phys. Lett. **90**, 263 107 (2007).
[19] O. Schumacher, S. Mendach, H. Welsch, A. Schramm, Ch. Heyn, and W. Hansen, Appl. Phys. Lett. **86**, 143 109 (2005).
[20] D. J. Thurmer, C. Deneke, Y. Mei, and O. G. Schmidt, Appl. Phys. Lett. **89**, 223 507 (2006).
[21] S. Mendach, O. Schumacher, H. Welsch, Ch. Heyn, W. Hansen, and M. Holz, Appl. Phys. Lett. **88**, 212 113 (2006).
[22] M. Grundmann, Appl. Phys. Lett. **83**, 2444 (2003).
[23] For example, M. Born and E. Wolf, *Principles of Optics* (Pergamon Press, Oxford, 1980).
[24] S. Zollner and D. Zarr, 2000 IEEE International Symposium on Compound Semiconductors (2000), p. 13.
[25] P. B. Johnson and R. W. Christy, Phys. Rev. B **6**, 4370 (1972).
[26] B. Wood, J. B. Pendry, and D. P. Tsai, Phys. Rev. B **74**, 115116 (2006).